DEFECT DETECTION AND QUALITY ASSESSMENT OF HARDWOOD LOGS: PART 1—ACOUSTIC IMPACT TEST AND WAVELET ANALYSIS[1]

Feng Xu
PhD Candidate
College of Information Science and Technology
Nanjing Forestry University
Nanjing, Jiangsu, China
E-mail: xufeng@njfu.com.cn

*Xiping Wang**†*
Research Forest Products Technologist, PhD
USDA Forest Service
Forest Products Laboratory
Madison, WI
E-mail: xwang@fs.fed.us

Ed Thomas
Research Computer Scientist
USDA Forest Service
Northern Research Station
Princeton, WV
E-mail: ethomas@fs.fed.us

*Yunfei Liu**
Professor
College of Information Science and Technology
Nanjing Forestry University
Nanjing, Jiangsu, China
E-mail: lyf@njfu.edu.cn

Brian K. Brashaw
Program Manager
E-mail: bbrashaw@fs.fed.us

Robert J. Ross
Project Leader
USDA Forest Service
Forest Products Laboratory
Madison, WI
E-mail: rjross@fs.fed.us

(Received January 2018)

Abstract. The objective of this study was to determine the technical feasibility of combining acoustic wave data with high-resolution laser scanning data to improve the accuracy of defect detection and quality assessment in

* Corresponding author
† SWST member
[1] This article was written and prepared by US Government employees on official time, and it is therefore in the public domain and not subject to copyright.

Wood and Fiber Science, 50(3), 2018, pp. 291-309
https://doi.org/10.22382/wfs-2018-029

hardwood logs. This article (Part 1) focused on exploring the potential of an acoustic impact testing method coupled with advanced waveform analysis to detect internal decay of hardwood logs and classify logs in terms of log quality and potential board grade yields. Twenty-one yellow-poplar (*Liriodendron tulipifera*) logs obtained from the Central Appalachian region were evaluated for internal soundness using an acoustic impact testing technique. These logs were then sawn into boards, and the boards were visually graded based on National Hardwood Lumber Association grading rules. The response signals of the logs from acoustic impact tests were analyzed through moment analysis and continuous wavelet transform to extract time-domain and frequency-domain parameters. The results indicated that the acoustic impact test coupled with wavelet analysis is a viable method to evaluate the internal soundness of hardwood logs. Log acoustic velocity alone was able to identify the very low-end logs that have the most severe internal rot or other unsound defects but failed to identify the logs with poor geometry that resulted in very low recovery. Time centroid, damping ratio, and combined time- and frequency-domain parameters were found effective in predicting log quality in terms of board grade yields. Log segregation based on time-domain (time centroid and ρ/T_c^2) and frequency-domain (damping ratio and E_d/ζ^2) parameters showed a positive correlation with the board grade yields.

Keywords: Acoustic velocity, board grade, damping ratio, impact test, log defects, dynamic MOE, time centroid, yellow-poplar.

INTRODUCTION

Internal defects in standing timbers and felled logs cause the U.S. wood industry millions of dollars in processing and reprocessing wood to keep defective portions from being included in end products. The economic loss caused by heartwood decay and other internal defects is most significant for hardwood trees and logs used to produce high-value appearance-grade products. For example, veneer logs typically cost 1.5-6 times that of Forest Service factory grade 1 sawlogs (Wiedenbeck et al 2003). Because of the exceptionally high prices paid for high-quality logs, undetected defects in hardwood logs can cause a substantial monetary loss to timber buyers and wood manufacturers. Early detection of internal defects in hardwood logs could provide a significant benefit to the industry by allowing accurate quality assessment and volume estimates, which would lead to optimal use of the hardwood resource.

Another important reason for early defect detection in hardwood logs is to remove logs from the processing stream that have little or no profitability. This concept is commonly known as the "break-even log" because processing a log with quality lower than the break-even log results in a loss for the company. Ideally, to realize target profit maximization, logs that give no real financial return from processing should be sold to other processors that can economically process these logs into products such as railroad ties, pallet lumber, pulp, or fuel.

Research in the field of nondestructive testing and evaluation of wood has resulted in an array of tools for detecting internal wood defects. Technologies such as X ray, computed tomography, and nuclear magnetic resonance offer cross-sectional images with sufficient detail, but they are not cost-effective for hardwood mills and are too slow to be considered suitable for on-line implementation (Wagner et al 1989; Chang 1992; Li et al 1996; Guddanti and Chang 1998; Bhandarkar et al 1999). As an alternative method, laser scanning has been investigated for detecting surface defects regarded as degrade defects by the visual grading rules. In addition, models were developed to predict internal defects based on external features (Thomas et al 2006, 2008). However, a system based entirely on log surface inspection may incorrectly predict internal quality. Some defects give the appearance of being solid or sound and effectively hide an unsound or rotten area, thereby reducing the accuracy of predicted internal product quality and value.

Acoustic wave methods use a mechanical impact to generate low-frequency stress waves that propagate longitudinally through a log and record the reverberation of the waves within the log. At the microstructure level, energy storage and dissipation properties of a log are controlled by orientation of wood cells and structural

composition, factors that contribute to stiffness and strength of wood. Such properties are observable as frequency of the wave reverberation and rate of wave attenuation. Research has shown that log acoustic measures can be used to predict the stiffness and strength of structural lumber that would be produced from the log (Aratake et al 1992; Aratake and Arima 1994; Ross et al 1997; Wang 2013). This research has opened the way for acoustic technology to be applied in mills for sorting and grading softwood logs for structural quality. Commercial acoustic tools are now accepted in the forest products industry for on-line quality control (structural lumber and veneer) and field or in-plant segregation of incoming softwood logs (Harris et al 2002; Carter et al 2005; Wang et al 2007, 2013; Gaunt 2012; Wang 2013; Murphy and Cown 2015). However, research on the use of the acoustic wave method for detecting internal defects in hardwood logs has been found to be very limited. In a mill study of assessing the stress level and potential wood quality of logs affected by oak decline, Wang et al (2009) acoustically tested 400 black and scarlet oak logs using an acoustic resonance tool. Principal component and canonical correlation analyses revealed that relationships do exist between log acoustic measurement and board grade yield, and between a linear combination of log acoustic velocity and diameter at breast height and a linear combination of board defect measurements. But, no effort has been made to explore new acoustic features beyond acoustic velocity to assess hardwood logs in terms of internal defects and board visual criteria.

Acoustic waves and laser scanning methods operate under different principles. Each addresses the weaknesses or inabilities of the other. The objective of this pilot study was to determine the technical feasibility of combining acoustic wave data with high-resolution laser scanning data to improve the accuracy of defect detection and quality evaluation in hardwood logs. The results of this research are reported in two parts. Part 1 (this report) explores the capabilities and limitations of an acoustic impact testing method coupled with advanced waveform analysis to detect internal defects of hardwood logs and classify logs in terms of potential board quality and grade yields. Part 2 will evaluate the effectiveness of using a combined acoustic and laser scanning system to rank hardwood logs and further improve the log segregation process.

MATERIALS AND METHODS

A random sample of 15 yellow-poplar (*Liriodendron tulipifera*) trees were harvested from a MeadWestVaco (Richmond, VA) leased and managed forest near Rupert, WV, in the Central Appalachian region in late January of 2015. Each tree was bucked to commercial lengths with three to five logs being cut from each tree, resulting in a total of 52 logs. Each log was tagged with a tree number and a log section code (A—butt log; B—2nd log; C—3rd log; D—4th log; and E—5th log). All logs were transported to the United States Department of Agriculture (USDA) Forest Service, Forestry Sciences Laboratory located in Princeton, WV. Visual observation showed that these logs ranged in quality level. Some logs had very obvious rot after bucking, some had deeply grown wounds with significant encapsulated decay pockets, and some were very high quality. The logs were stored outside and exposed to winter weather for about 1 mo before the acoustic testing.

Acoustic Impact Test

One week before the acoustic impact test, the logs were moved into the heated laboratory building to allow the wood to thaw and reach room temperature. Each log was first put on a rack for physical diagramming of surface defect indicators and high-resolution laser scanning (detailed procedures are outlined in Part 2 of this series). Each log was also weighed using a crane scale (LHS4000a, ADAM Equipment, Inc., Oxford, CT) by lifting the log up through a log loader. The crane scale has a capacity of 2000 kg and is accurate to the nearest 0.5 kg. Log density was determined based on the gross weight and the exact volume derived from the 3D laser scanning data.

Logs were then acoustically tested on the ground to obtain acoustic parameters for potential

detection of internal defects. Acoustic impact tests were conducted in two different ways: 1) using a resonance-based acoustic tool to directly measure the acoustic velocity of each log and 2) using a laboratory impact testing system to obtain and record the response signals from each log following a mechanical impact. All acoustic tests were conducted under conditions of 21°C and 50% relative humidity (RH).

A hand-held resonance acoustic tool (Hitman HM200, Fiber-gen, Inc., Auckland, New Zealand) was used to directly measure the acoustic velocity of each log. Following a hammer impact, the HM200 tool immediately processes the received acoustic signals through the Fast Fourier Transform program built into the tool and calculates log acoustic velocity (V) based on the resonant frequency and log length:

$$V = 2f_n L/n, \quad (1)$$

where f_n is the nth harmonic frequency (Hz) of the response signal, L is the full length of a log (m), and n is the order of harmonic frequency.

To ensure the accuracy of log velocity measurement, three high-confidence (indication of good signals) velocity values were obtained from each log. The average velocity value was calculated for each log and used in data analysis.

To collect the response signals from each log, a sensor probe (Fakopp spike sensor, Fakopp Enterprise Bt., Agfalva, Hungary) was inserted into the end grain at the log end (close to the center). The impact acoustic waves were generated through a 5.44-kg sledge hammer blow on the opposing end, and the response signals were recorded through the data acquisition card (NI 5132) connected to the laptop, with a sampling frequency of 20 kHz and a sampling length of 1000 points. Three replicate signals were obtained from each log.

Sawing and Visual Grading

After acoustic testing, 21 logs were selected and sawn into 29-mm-thick boards using a portable sawmill. The reason of not sawing all 52 logs was because we only had limited budget at the time of this study and the time window available for the sawing process was also limited. This subsample of logs was systematically selected based on visual assessment and resonant acoustic testing results such that they represent the quality range of the 52 logs. The sawing was performed by an experienced sawyer who worked to maximize the yield and value of the lumber with respect to the National Hardwood Lumber Association (NHLA) rules (NHLA 2015). The general sawing strategy was to open the log on the best face and rotate the log when the face grade of the cant dropped. Some wood moisture samples were cut during the sawing process for determining moisture contents of the logs using the oven-dry method.

The resulting boards were visually graded according to NHLA rules (NHLA 2015). The NHLA rules are based on the size and number of cuttings (pieces) that can be obtained from a board when it is cut up and used in the manufacture of a hardwood product. Therefore, each grade provides a measurable percentage of clear, defect-free wood. The board grades determined based on NHLA rules include high grades (FAS—First and Second, F1F—FAS One Face, and Select), common grades (No. 1 Common, No. 2 Common, and No. 3 Common), and below grade (BG).

Extraction of Acoustic Parameters

In addition to the acoustic velocity directly measured on each log, physical and acoustic parameters of the subsample of logs were obtained and evaluated for their potential to predict the soundness of the logs and grade yields of the resulting boards. The predicting parameters we examined included acoustic velocity (V), dynamic MOE (E_d), time centroid (T_c), and damping ratio (ζ), as well as two combined parameters of the response signals.

The acoustic parameters were extracted based on the following procedures: 1) compute dynamic MOE of the logs based on log density and

measured log velocity; 2) determine time centroid (T_c) of the response signals through first moment analysis; 3) perform continuous wavelet transform (CWT) of the response signals and compute the wavelet ridge by maximizing the modulus of wavelet skeleton at each time instant; 4) compute instantaneous natural frequency (f_i) and damping ratio (ζ_i) according to the wavelet ridge and skeleton.

Dynamic MOE (E_d). Modulus of elasticity of a log is a global property that can be readily estimated based on the one-dimensional wave equation:

$$E_d = \rho V^2, \tag{2}$$

where ρ is gross density of a log (green, at the time of acoustic testing) and V is the measured log velocity.

Time centroid (T_c). Time centroid, sometimes referred to as "mean time," represents the time when the bulk of the signal is received. Mathematically, T_c is obtained by dividing the first moment of the signal by the zeroth moment of the signal:

$$T_c = \frac{\sum_{i=1}^{N} |A_i| t_i}{\sum_{i=1}^{N} |A_i|}, \tag{3}$$

where N is the number of time samples, A_i is the amplitude of the ith time step, and t_i is the time at the ith time step.

In general, when a signal is excited and transmitted in a flawless medium, most of its energy is typically located in the beginning of the signal waveform. Reflection and mode changes of the signal often come from the boundaries and material flaws, causing skewing of the signal in the time domain. As a form of the first moment analysis, time centroid has been widely used to characterize the damage or deterioration of materials (Tiitta et al 1998; Bayissa et al 2008).

Damping identification using a wavelet transform. Damping, often expressed by the damping ratio, is the dissipation of vibration

Table 1. Dimensional and physical measures of the yellow-poplar logs.

Log no.	Length (m)	Diameter (cm)			Weight (kg)	Density (kg/m^3)	Sweep (cm)	Debarked volume (m^3)
		Large end	Small end	Avg.				
1C	3.47	46.7	43.1	47.3	419.0	685.4	4.1	0.519
2A	3.99	51.2	51.2	49.5	537.1	672.5	3.5	0.682
3A	3.99	59.2	52.0	53.9	827.6	885.7	2.7	0.801
3B	4.63	50.9	50.9	52.8	821.7	783.5	2.2	0.897
3D	5.00	38.1	35.1	36.4	388.2	729.5	5.4	0.441
4B	4.48	48.4	47.1	47.6	498.0	610.9	2.4	0.692
4C	5.12	42.7	39.1	40.7	420.4	614.5	2.1	0.574
4E	4.27	32.4	32.4	32.6	167.1	497.1	1.3	0.273
5A	4.11	48.4	43.1	45.2	548.9	828.8	2.0	0.559
5B	3.38	42.6	41.1	41.7	363.7	767.6	4.3	0.399
5D	3.38	37.9	37.9	37.9	291.0	760.1	5.3	0.319
5E	4.08	35.8	35.8	35.8	311.4	759.8	4.3	0.339
8A	3.81	36.2	34.5	35.7	286.9	735.4	4.2	0.324
11A	3.60	53.4	51.6	54.0	675.1	785.9	3.9	0.737
11B	2.90	52.9	52.9	52.1	643.8	810.1	3.1	0.550
11C	3.47	51.1	46.1	48.2	522.6	800.3	6.3	0.556
12D	5.03	43.4	38.4	40.5	548.4	827.0	4.6	0.556
14B	5.18	59.9	58.5	57.9	1202.6	831.0	2.3	1.246
14C	3.47	46.4	42.7	44.8	459.4	827.4	3.7	0.469
15A	4.91	44.1	37.5	39.2	474.9	780.3	4.0	0.509
15B	4.42	37.1	37.1	36.8	360.0	740.5	3.2	0.405

Table 2. Summary of the acoustic measures of the yellow-poplar logs.[a]

Log no.	V (km/s)	E_d (GPa)	f (Hz)	T_c ($\times 10^{-2}$ s)	ζ ($\times 10^{-2}$)	ρ/T_c^2 ($\times 10^6$ kg/m^3 s^{-2})	E_d/ζ^2 ($\times 10^3$ GPa)
1C	3.34	7.65	521.7	1.74	3.59	2.26	5.93
2A	3.37	7.65	413.8	1.64	3.43	2.51	6.52
3A	3.04	8.18	382.2	1.47	3.61	4.10	6.27
3B	3.05	7.29	344.8	1.93	4.25	2.10	4.04
3D	3.27	7.81	331.5	2.08	4.26	1.68	4.31
4B	3.83	8.98	425.5	1.90	4.12	1.70	5.29
4C	3.78	8.79	372.7	1.88	4.41	1.73	4.51
4E	3.59	6.42	425.5	1.98	3.73	1.26	4.61
5A	3.65	11.05	447.8	1.41	3.16	4.14	11.04
5B	3.88	11.57	576.9	1.44	3.02	3.71	12.71
5D	3.76	10.72	560.8	1.75	3.16	2.50	10.76
5E	3.67	10.21	458.0	1.57	3.83	3.07	6.95
8A	2.91	6.22	389.6	1.80	3.88	2.27	4.14
11A	3.38	8.98	480.0	1.48	4.17	3.60	5.17
11B	2.93	6.95	560.8	1.21	3.75	5.50	6.08
11C	3.32	8.85	476.2	1.51	4.53	3.49	4.30
12D	3.23	8.64	319.2	2.04	4.27	1.98	4.75
14B	3.30	9.06	317.5	1.69	4.06	2.91	5.50
14C	2.98	7.35	428.6	1.88	4.14	2.34	4.29
15A	3.63	10.28	387.1	1.53	3.16	3.31	10.27
15B	3.73	10.31	419.6	1.70	4.13	2.54	6.06

[a] V, acoustic velocity; E_d, dynamic modulus of elasticity; f, fundamental frequency; T_c, time centroid; ζ, damping ratio; ρ, log density.

energy in a material. Damping is an important factor in characterizing material properties. However, the determination of damping is complex, depending on test procedures and data analysis. In this report, the damping ratio of the response signal was estimated through CWT. The theoretical background of CWT and the procedures to determine the instantaneous frequency and damping ratio of the logs through wavelet analysis are presented in the Appendix. Based on the wavelet ridge and skeleton computed for each time instant, instantaneous frequency f_i and damping ratio ζ_i of each log can be derived by solving the following equation:

$$\begin{cases} \dfrac{\mathrm{d}\ln B_i(t)}{\mathrm{d}t} = \dfrac{1}{B_i(t)}\dfrac{\mathrm{d}B_i(t)}{\mathrm{d}t} = -2\pi\zeta_i f_i \\ \dfrac{\mathrm{d}\phi_i(t)}{\mathrm{d}t} = 2\pi f_{di} = 2\pi f_i\sqrt{1-\zeta_i^2} \end{cases}. \quad (4)$$

Flowing signal processing, an average value for each individual acoustic parameter (dynamic MOE, time centroid, and damping ratio) was obtained for each log and used in subsequent data analysis.

Data Analysis

The research approach we adopted in this study was a practical one, that is to saw the logs into boards following acoustic impact test and laser scanning and use the board grade data as the log quality indication, which is the case in mill production. One of the limitations of this approach is that we were not able to obtain quantitative data of actual internal defects on the boards and logs, thus a linear analysis was not possible. To evaluate the effectiveness of the acoustic parameters as quality predictors, we analyzed the characteristics of each possible predicting parameter and determined the relationships between the acoustic parameters (individual and combinations) of the logs and the grade yield of the boards sawn from the logs. For this purpose, the 21 yellow-poplar logs were ranked and segregated into three acoustic classes (high, medium, and low quality sort) based on the following sorting parameters: 1) acoustic velocity (V), 2) time centroid (T_c), 3) damping ratio (ζ), 4) combination of density (ρ) and time centroid (T_c), and 5) combination of dynamic MOE (E_d) and damping ratio (ζ). In general, the class

thresholds were evenly set across the determined range of each parameter. However, minor adjustments were made when the observed data showed distinct uneven distribution and also for rounding the values to even numbers when necessary. The resulting sample size of each log class ranged from 5 to 9 logs. It should be pointed out that the sample size of this study was considered small, thus the ranges of the acoustic parameters observed on the sample logs were limited, and the parameter thresholds presented in this article for segregating logs are indicative and preliminary.

RESULTS AND DISCUSSION

Table 1 shows the dimensional and physical measures of 21 selected yellow-poplar logs. The logs measured 2.9-5.18 m in length with an average diameter ranging from 35.7 to 57.9 cm. It is noted that on some logs, the small end is larger than the average diameter. In most cases, this is because of a large knot being present at the end of the log. In other cases, abnormalities such as gouges or multiple knots in the center of the log skew the average diameter.

Table 2 summarizes the acoustic measures of 21 selected yellow-poplar logs. Acoustic impact testing of the logs took place in early March, 1 mo after harvesting. The moisture contents of these wood samples were found to be 45-60%, which confirmed that the logs were in green condition (well above the FSP of 30% MC) at the time of acoustic testing. Therefore, all acoustic parameters discussed in this report are considered green log parameters.

Table 3 shows the sawing results (board volume, cant volume, board grade yield, and recovery rate) of 21 selected logs. A total of 294 boards were sawn from the sample logs, with the width ranging from 12 to 41 cm and length ranging from 2.74 to 4.88 m. The board recovery rate ranged from 26.5% for log 5E to 64.6% for log 3A. The high-grade boards are a combination of FAS, F1F, and Select grades. The below-grade boards were also included in the table for the purpose of log quality analysis.

Table 3. Sawing results of the yellow-poplar logs.

	Volume (m^3)			Grade yield (m^3)					Recovery (%)	
Log no.	Debarked	Board	Cant	High[a]	1C	2C	3C	BG	Total[b]	Board
1C	0.519	0.250	0.081	0.040	0.068	0.099	0.042	0	63.9	48.2
2A	0.682	0.373	0.076	0.326	0.019	0.017	0	0.012	65.8	54.7
3A	0.801	0.517	0.070	0.441	0.045	0	0.012	0.019	73.3	64.6
3B	0.897	0.467	0.083	0.139	0.286	0.014	0.014	0.014	61.3	52.1
3D	0.441	0.156	0.080	0.071	0.038	0.047	0	0	53.5	35.3
4B	0.692	0.371	0.090	0.076	0.132	0.097	0.066	0	66.6	53.5
4C	0.574	0.274	0.104	0.054	0.165	0.054	0	0	65.8	47.7
4E	0.273	0.085	0.066	0	0.017	0.028	0.040	0	55.5	31.1
5A	0.559	0.323	0.050	0.304	0.019	0	0	0	66.8	57.8
5B	0.399	0.205	0.059	0.144	0.061	0	0	0	66.4	51.5
5D	0.319	0.085	0.079	0	0.028	0.028	0.028	0	51.4	26.6
5E	0.339	0.090	0.097	0	0.024	0.066	0	0	55.2	26.5
8A	0.324	0.142	0.074	0.090	0.014	0.009	0	0.028	66.5	43.8
11A	0.737	0.378	0.080	0.208	0.135	0.012	0.024	0	62.1	51.3
11B	0.550	0.297	0.073	0.179	0.076	0.042	0	0	67.3	54.0
11C	0.556	0.264	0.140	0.054	0.085	0.109	0.017	0	72.7	47.6
12D	0.556	0.234	0.111	0.012	0.111	0.111	0	0	61.9	42.0
14B	1.246	0.684	0.074	0.453	0.137	0.094	0	0	60.8	54.9
14C	0.469	0.236	0.071	0.045	0.047	0.076	0.068	0	65.5	50.3
15A	0.509	0.231	0.102	0.127	0.035	0.068	0	0	65.5	45.5
15B	0.405	0.201	0.063	0.076	0.092	0.021	0	0.012	65.2	49.5

[a] High includes grade First and Seconds, F1F, and Select.
[b] Total, includes boards and cant.
BG, below grade.

Acoustic Velocity

Acoustic velocity of the 21 selected yellow-poplar logs ranged from 2.91 to 3.88 km/s, which matches the velocity range of the 52 logs bucked from the 15 randomly selected trees. We ranked the 21 selected logs by acoustic velocity in descending order and segregated them into three groups based on the following velocity ranges:

Group 1 (G1): $3.60 \leq V < 3.90$ km/s (high-quality class)
Group 2 (G2): $3.30 \leq V < 3.60$ km/s (medium-quality class)
Group 3 (G3): $2.90 \leq V < 3.30$ km/s (low-quality class)

The acoustic velocity class of the logs was then associated with the board grades determined based on the NHLA grading rules. Figure 1 shows the distributions of board grade yield in relation to log acoustic velocity classes. Three log groups had almost the same volume recovery, 63.9% for G1, 63.6% for G2, and 64.6% for G3. Among the boards recovered, three log groups showed similar grade distribution, highest yield for the high-grade boards and decreasing yields for 1 Common, 2 Common, 3 Common, and BG boards. The log acoustic class did not show a direct correlation with the board grade yield. In fact, the medium-velocity logs (G2) yielded the most high-grade boards (53.1%), and the low-velocity logs yielded 47.7% high-grade boards, even higher than the high-velocity logs (43.9%). In the BG level only, the log acoustic class showed a positive trend; that is, BG boards increased as log velocity decreased. But, the BG boards only counted for 0.6-3% among all the boards. Therefore, acoustic velocity does not appear to be a meaningful predictor in log group rating.

In physics, the velocity of stress waves propagating through a log depends on both stiffness and mass density of the log. The existence of small defects inside a log may not affect the global stiffness of the log but could have a significant

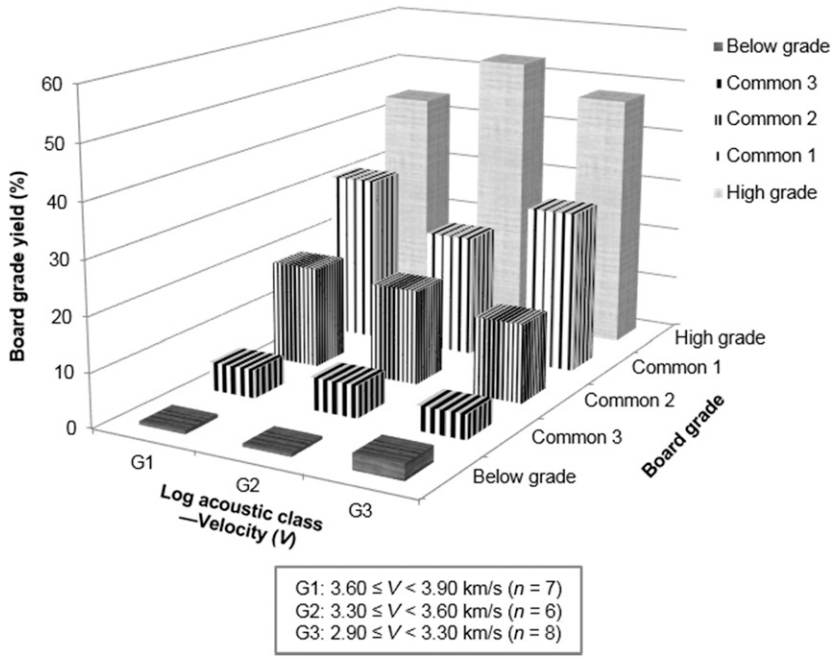

Figure 1. Distribution of yellow-poplar board grade yields in relation to log acoustic classes segregated based on acoustic velocity.

impact on the board grades according to the hardwood visual grading rules. In addition, it is understood that longitudinal waves traveling along the length of a material are not sensitive to the presence of small sound defects because the waves can bypass small defects without causing significant changes in overall propagation path. This could be a major contributor to the poor correlation between log velocity class and board grade yield.

Conversely, the presence of significant internal decay or major structural defects inside a log could effectively decrease wood density, significantly impact wave propagation behavior, and thus result in abnormally low acoustic velocity (Wang et al 2009). Based on analysis of log velocity distribution, five logs (8A, 11B, 14C, 3A, and 3B) were identified as having unusually low velocities (2.91-3.05 km/s). The sawing results confirmed that these logs either had internal rot, incipient decay, or missing wood (logs 3A, 3B, 11B, and 14C) or had other structural defects that caused a significant downgrade in the sawn boards (log 8A). Therefore, acoustic velocity was still effective in identifying logs with severe internal rot or other unsound defects.

Another important observation was that acoustic velocity failed to identify two small diameter logs (5D and 5E) that had a significant amount of sweep (up to 5.3 cm) and resulted in the lowest board recovery (26.5%) among the sample logs. It appeared that wave propagation was not very sensitive to the longitudinal distortion, at least to the extent of the sweep or crook observed in the yellow-poplar sample logs.

Time Centroid

Figure 2 shows the time signals (absolute amplitude) and time centroid curves of the response signals from two yellow-poplar logs, one from log 5B (considered sound and good quality) and one from log 12D (considered a low-quality log). As we examined the time centroid curves (dot lines) of these two different logs, we found that the T_c of the good quality log (Fig 2a) exhibited a steep slope in the beginning of the signal,

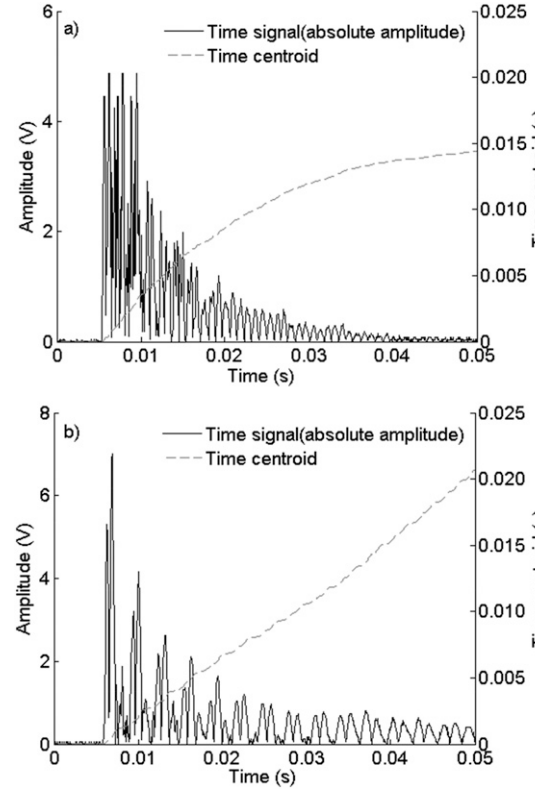

Figure 2. Typical time signals and time centroid curves of response signals received from yellow-poplar logs (a) Log 5B; (b) Log 12D.

indicating a fast energy transmission. Then, the T_c curve became flat at the end of the signal, indicating that the energy gradually dissipated. However, the low-quality log (Fig 2b) showed different characteristics in the T_c curve. The slope of the curve remained almost constant, indicating that the signal energy was dissipated more quickly than that of the high-quality log.

The time centroids of the response signals obtained from the 21 selected logs are listed in Table 2. We ranked the logs by T_c in ascending order and segregated them into three groups based on the following evenly divided T_c ranges:

G1: $1.20 \leq T_c < 1.50 \times 10^{-2}$ s (high-quality class)

G2: $1.50 \leq T_c < 1.80 \times 10^{-2}$ s (medium-quality class)

G3: $1.80 \leq T_c < 2.10 \times 10^{-2}$ s (low-quality class)

The lower the T_c value is, the greater the energy at the beginning of the response signal, which then correlates to better quality with higher grade yield.

Figure 3 shows the distributions of board grade yield in relation to log time-centroid classes. A direct correlation was found between board grade yield and log time-centroid among the three log classes. As the log time-centroid increased, the yield of high-grade boards decreased significantly, with a change from 74.2% for G1 to 50.3% for G2 ($\alpha = 0.05$) and 21.8% for G3 ($\alpha = 0.01$). Meanwhile, the yields of the following three lower grades (1, 2, and 3 common) increased significantly ($\alpha = 0.05$). These two opposite time-centroid trends reflected distinct differences between high-quality boards with no or few defects and common-grade boards with some defects such as sound knots, unsound knots, or knot clusters and incipient decay.

Damping Ratio

To estimate damping ratio (ζ) of the response signals, a CWT was performed to the time signals using the Morlet wavelet function. As examples, Fig 4 shows the response signal of a good quality log (log 5B) and the corresponding CWT analysis, and Fig 5 shows the response signal of a low-quality log (log 12D) and the corresponding CWT analysis. The wavelet modulus obtained is shown in Figs 4b and 5b (two-dimensional contour map) and Figs 4c and 5c (three-dimensional image). The wavelet ridge and skeleton were subsequently calculated from the wavelet modulus and are shown in Figs 4b and 5b as a red line and in Figs 4c and 5c as a black line, respectively. Figures 4d and 5d show the instantaneous frequency, damping ratio, and damping ratio fitting curve (high-order polynomial fitting).

The instantaneous frequency we obtained was the instantaneous natural frequency; therefore, the corresponding damping ratio was the first-order damping ratio. For log 5B, a high-quality log proved by sawing results, the intrinsic frequency

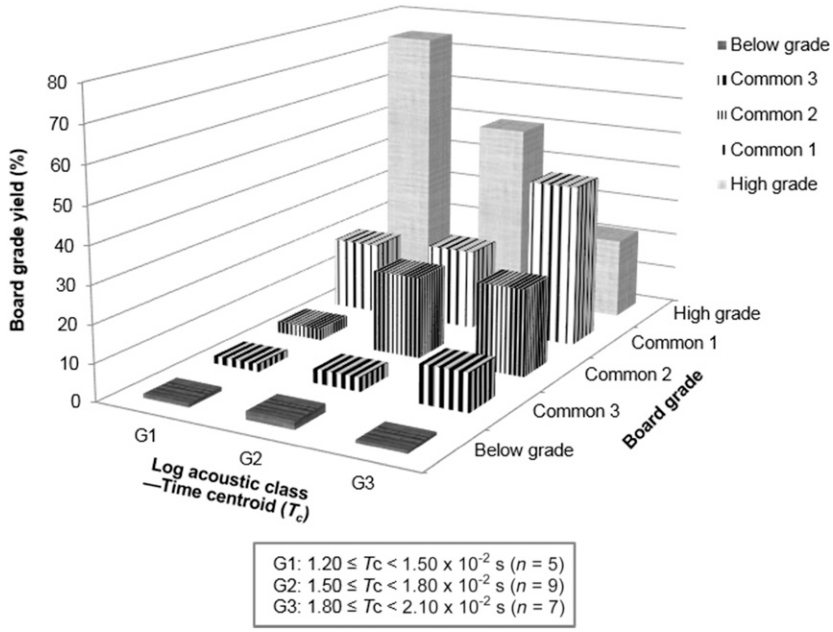

Figure 3. Distributions of yellow-poplar board grade yield in relation to log acoustic classes segregated based on time centroid (T_c).

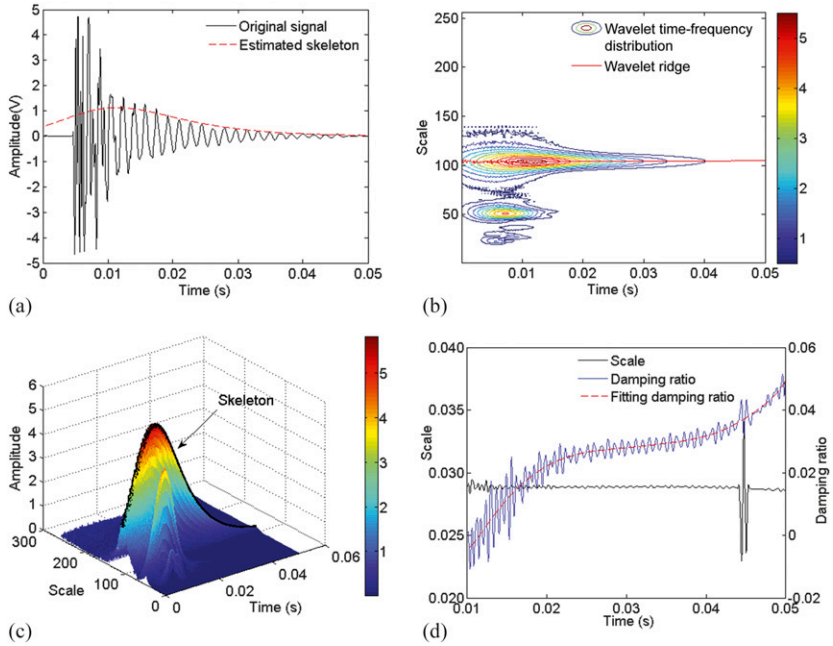

Figure 4. Response signal of yellow-poplar log 5B (high-quality log) and CWT analysis. (a) time-domain signal and its envelope (red dotted line); (b) time-scale distribution of signal's CWT and wavelet ridge (red line); (c) time-scale distribution of signal's CWT (3D) and wavelet skeleton; and (d) instantaneous frequency (scale), damping ratio, and damping ratio fitting curve of the signal.

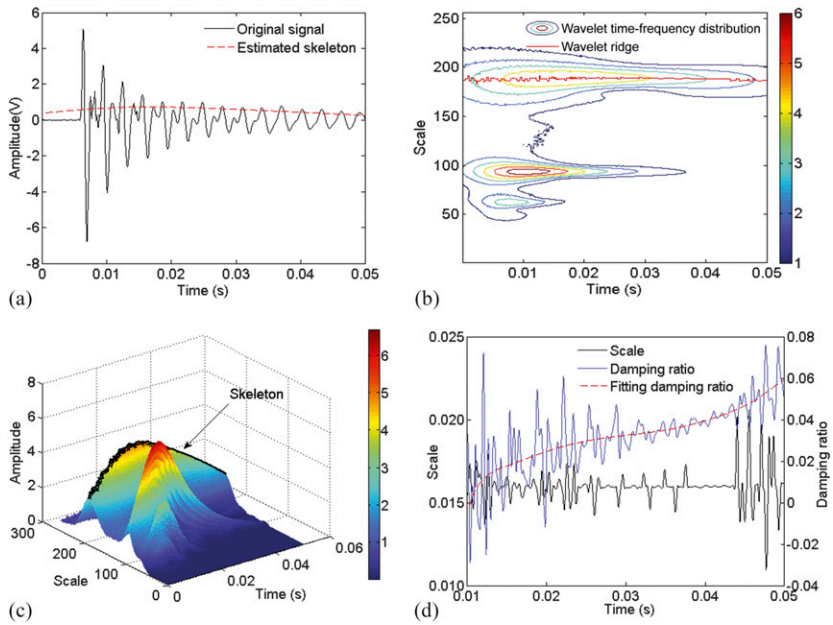

Figure 5. Response signal of yellow-poplar log 12D (low-quality log) and CWT analysis. (a) time-domain signal and its envelope (red dotted line); (b) time-scale distribution of signal's CWT and wavelet ridge (red line); (c) time-scale distribution of signal's CWT (3D) and wavelet skeleton; and (d) instantaneous frequency (scale), damping ratio, and damping ratio fitting curve of the signal.

did not show much change within a finite duration of the analyzed signal (sampling points: 300-900), indicating that the reflection and refraction of the acoustic signal that are typically associated with internal defects in a material did not occur. Consequently, a frequency conversion phenomenon was not observed. As a result, the damping ratio estimated from the instantaneous frequency did not have much variation. In the case of log 12D, a low-quality log indicated by sawing results, variation of the damping ratio was found prominent as a result of existing internal defects (decay, sound and unsound knots, and heavy distortion) revealed by the sawing results.

Damping ratio increased with the existence of internal damage because the additional surfaces created in damage areas increased the dissipation of the acoustic energy. This increase in damping ratio can be used as a measure of the extent of internal defects in a log. Therefore, we classified the logs into three classes based on the following damping ratio ranges, which were approximately evenly divided across the range:

G1: $3.00 \leq \zeta < 3.50 \times 10^{-2}$ (high-quality class)
G2: $3.50 \leq \zeta < 4.10 \times 10^{-2}$ (medium-quality class)
G3: $4.10 \leq \zeta < 4.60 \times 10^{-2}$ (low-quality class)

Figure 6 shows the distribution of board grade yield in relation to log damping ratio classes. For the logs in the low damping ratio class G1 (high-quality sort), the high-grade boards accounted for about 74.1% and low-grade boards (including 2 common, 3 common, and BG) were only 12.6%. By contrast, for the logs in the high damping ratio class G3 (low-quality sort), the high-grade boards only accounted for 28.5%, a significant decrease compared with the G1 class; whereas the low-grade boards increased to 29.3%, a significant increase compared with the G1 class. Similarly to time centroid, two opposite trends of board grade yield in damping ratio classes reflect distinct differences in the quality of the resulting boards. As for medium-quality logs, all of their lumber grade yields were located between that of high-quality and low-quality logs.

Combined Parameter ρ/T_c^2

Wood density (ρ) is usually not considered a factor in hardwood visual grading, but it is relevant in assessing the soundness of hardwood logs. The existence of any significant internal rot in a log may effectively decrease the gross density of the log because of the loss of wood fibers. Wood density is also interrelated to acoustic wave propagation based on the one-dimensional wave theory, in which acoustic velocity is dependent on MOE and density. In this study, wood density data of the logs were combined with acoustic measures for multiparameter analysis.

After examining various possible combinations, a new parameter, ρ/T_c^2, derived from gross density of a log and the time centroid of the response signal, was found to be an effective predictor of log quality. Figure 7 shows the distribution of board grade yield in relation to log classes segregated based on the combined parameter ρ/T_c^2. Similarly to time centroid log classification, the yellow-poplar logs were divided into three classes according to the following ρ/T_c^2 ranges:

G1: $3.70 \leq \rho/T_c^2 < 5.50 \times 10^6$ kg/m^3 s^{-2} (high-quality class)
G2: $2.40 \leq \rho/T_c^2 < 3.70 \times 10^6$ kg/m^3 s^{-2} (medium-quality class)
G3: $1.25 \leq \rho/T_c^2 < 2.40 \times 10^6$ kg/m^3 s^{-2} (low-quality class)

There was a clear trend of increasing yield of high-quality boards as log class changed from low to high values of ρ/T_c^2. For the high-quality log class G1 with ρ/T_c^2 in the range of 3.70-5.50 $\times$ 10^6, the amount of high-grade boards reached almost 80%; whereas 1 Common and 2 Common had about 14.9% and 3.2%, respectively, 3 Common and BG accounted for only 2.3% combined. For the low-quality log class G3 with ρ/T_c^2 in the range of 1.25-2.40 $\times$ 10^6, high-grade boards only accounted for 23.8%, a significant decrease compared with that of class G1 ($\alpha = 0.01$); 1 Common accounted for 39.7% and the lower grade boards (2 common, 3 common, and BG combined) accounted for 36.5%, a significant increase compared with the

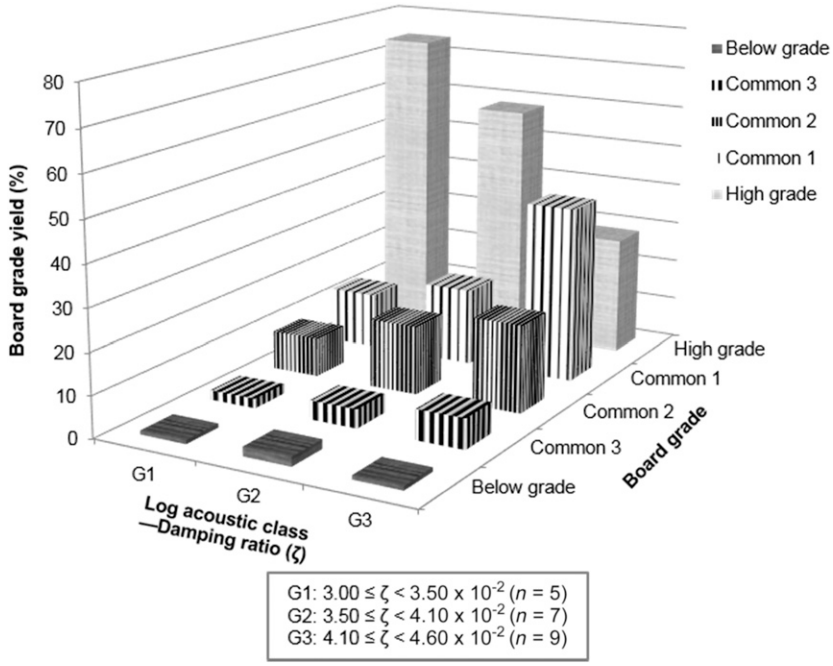

Figure 6. Distributions of yellow-poplar board grade yield in relation to log acoustic classes segregated based on damping ratio (ζ).

G1 class ($\alpha = 0.01$). As for the log class G2 with medium ρ/T_c^2, the grade yields of the resulting boards fell between the high and low ρ/T_c^2 classes.

Combined Parameter E_d/ζ^2

Modulus of elasticity or stiffness of wood is an important property in machine stress grading of structural timber. It is also a key property for determining the quality of laminated veneer lumber and other engineered wood products. Although it is not usually measured and monitored in hardwood log sawing process, the stiffness of a log, as a global parameter, can be affected by the soundness (decay presence) or internal structural defects (knots, cracks, grain distortions, etc.) of a log. In this study, dynamic MOE (E_d) of each log was determined using acoustic velocity and log gross density. The parameter E_d was then combined with damping ratio ζ to form a new parameter E_d/ζ^2 as a quality predictor.

Figure 8 shows the distribution of board grade yield in relation to log E_d/ζ^2 class. Similarly, the yellow-poplar logs were divided into three classes according to the following E_d/ζ^2 ranges:

G1: $6.50 \leq E_d/\zeta^2 < 12.80 \times 10^3$ GPa (high-quality class)
G2: $4.80 \leq E_d/\zeta^2 < 6.50 \times 10^3$ GPa (medium-quality class)
G3: $4.00 \leq E_d/\zeta^2 < 4.80 \times 10^3$ GPa (low-quality class)

The data show a clear trend of increasing yield of high-quality boards as log class changed from low to high values of E_d/ζ^2. For the high-quality log class G1, high-grade boards reached 69.0%, whereas 1 Common and 2 Common had 14.3% and 13.7%, respectively. 3 Common and BG accounted for only 3.1% combined. For the low-quality log class G3, high-grade boards only accounted for 25.0%, a significant decrease compared with the G1 class ($\alpha = 0.05$); 1 Common accounted for 41.0% and the lower grade boards (2 Common, 3 Common, and BG

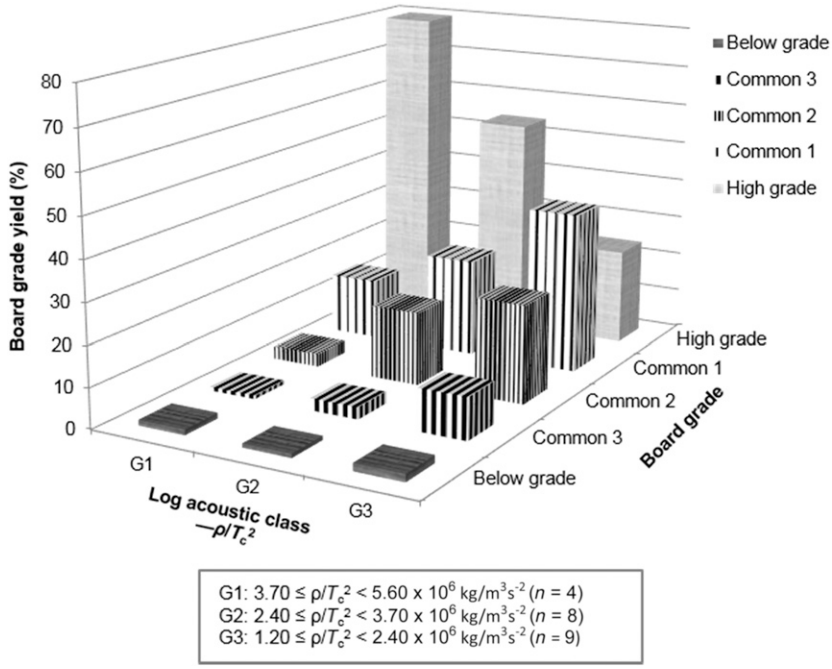

Figure 7. Distributions of yellow-poplar board grade yield in relation to log acoustic classes segregated based on ρ/T_c^2.

combined) accounted for 33.9%, both a significant increase compared with the G1 log class. As for the log class G2 with medium E_d/ζ^2, grade yields of the resulting boards fell between the high and low E_d/ζ^2 classes.

CONCLUSIONS

Acoustic impact test coupled with advanced waveform analysis was investigated as a new method for segregating hardwood logs in terms of internal soundness and potential board grade yields. The acoustic parameters examined included log acoustic velocity, time centroid, damping ratio, and two combined parameters, ρ/T_c^2 and E_d/ζ^2. Based on the results obtained from this study, the following conclusions can be drawn:

1. Log classes based on acoustic velocity did not show a clear direct correlation with board grade yields, but acoustic velocity was able to identify the very low-end logs that had the most severe internal rot or other unsound defects.
2. Acoustic velocity was not sensitive to longitudinal distortion of hardwood logs and therefore failed to identify logs with significant sweep or crook that resulted in very low board recovery.
3. Log classes based on time-domain (time centroid and ρ/T_c^2) and frequency-domain (damping ratio and E_d/ζ^2) parameters showed positive correlations with the board grade yields. The mechanism of each parameter associated with various unsound defects of logs are not yet fully understood, but each parameter has its strengths and weaknesses. Given the inherent great variability of internal defects in hardwood logs, all acoustic parameters resulting from impact testing should be considered in defect diagnosis to make an optimal sorting decision.
4. Because of the small sample size of this study, the distinction of log classes with the group thresholds presented in this article is indicative and preliminary. A production trial with a larger sample size is needed to further validate the effectiveness of the acoustic

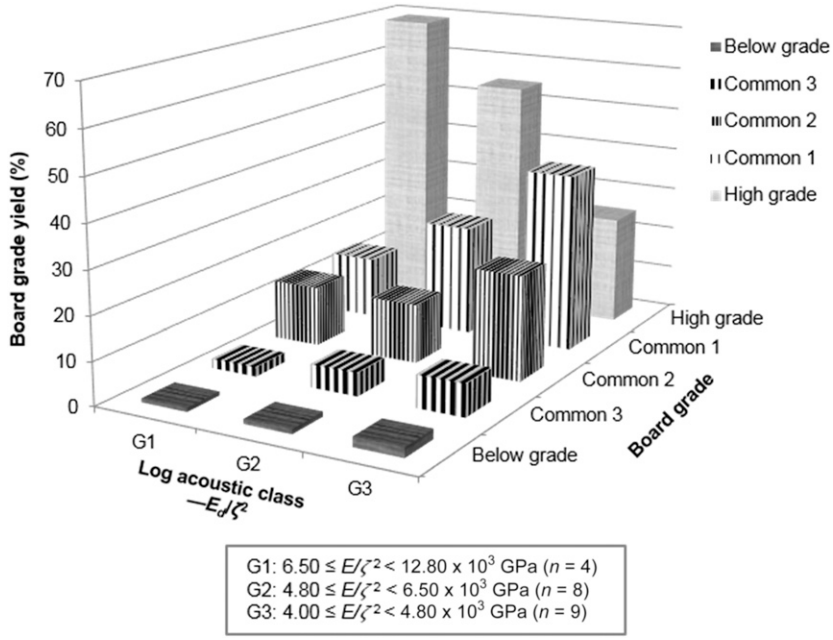

Figure 8. Distributions of yellow-poplar board grade yield in relation to log acoustic classes segregated based on E/ζ^2.

parameters and to determine practical log sorting criteria that will result in optimal use of the hardwood resource.

ACKNOWLEDGMENTS

This project was conducted under the cooperative research agreement (14-JV-11111133-089) between the Natural Resources Research Institute of the University of Minnesota Duluth and the USDA Forest Service, Forest Products Laboratory. Mr. Feng Xu's participation in this project was supported by the Priority Academic Program Development of Jiangsu Higher Education Institutions and the Nanjing Forestry University Innovation Grant for Outstanding PhD Dissertations (grant no. 163070682). We thank Neal Bennett and Deborah Conner for their technical assistance during the project.

REFERENCES

Aratake S, Arima T (1994) Estimation of modulus of rupture (MOR) and modulus of elasticity (MOE) of lumber using higher natural frequency of log in pile of logs II—Possibility of application for Sugi square lumber with pith. Mokuzai Gakkaishi 40(9):1003-1007.

Aratake S, Arima T, Sakoda T, Nakamura Y (1992) Estimation of modulus of rupture (MOR) and modulus of elasticity (MOE) of lumber using higher natural frequency of log in pile of logs—Possibility of application for Sugi scaffolding board. Mokuzai Gakkaishi 38(11):995-1001.

Bayissa WL, Haritos N, Thelandersson S (2008) Vibration-based structural damage identification using wavelet transform. Mech Syst Signal Process 22(5):1194-1215.

Bhandarkar S, Faust T, Tang M (1999) CATALOG: A system for detection and rendering of internal log defects using computer tomography. Mach Vis Appl 11(4): 171-190.

Carmona R, Hwang W, Torrésani B (1998) Practical time-frequency analysis: Gabor and wavelet transforms, with an implementation in S, 1st edition. Academic Press, Inc., San Diego, CA. 490 pp.

Carter P, Briggs D, Ross RJ, Wang X (2005) Acoustic testing to enhance western forest values and meet customer wood quality needs. PNW-GTR642. USDA Forest Service, Pacific Northwest Research Station, Portland, OR. pp. 121-129.

Chang S (1992) External and internal defect detection to optimize cutting of hardwood logs and lumber. Transferring Technologies for Industry No. 3. U.S. Department of Agriculture, National Agriculture Library, Beltsville, MD. 24 pp.

Delprat N, Escudié B, Guillemain P, Kronland-Martinet R, Tchamitchian P, Torrésani B (1992) Asymptotic wavelet

and Gabor analysis: Extraction of instantaneous frequencies. IEEE Trans Inf Theory 38(2):644-664.
Gaunt D (2012) A revolution in structural timber grading in World Conference on Timber Engineering, July 16-19, 2012, Auckland, New Zealand. 8 pp.
Grossmann A, Morlet J (1984) Decomposition of hardy functions into square integrable wavelets of constant shape. SIAM J Math Anal 15:723-736.
Guddanti S, Chang S (1998) Replicating sawmill sawing with topsaw using CT images of a full length hardwood log. Forest Prod J 48(1):72-75.
Harris P, Petherick R, Andrews M (2002) Acoustic resonance tools. Pages 195-201 *in* Proc. 13th International Symposium on Nondestructive Testing of Wood, August 19-21, 2002, Berkeley, CA. Forest Products Society, Madison, WI.
Kronland-Martinet R, Morlet J, Grossmann A (1987) Analysis of sound patterns through wavelet transforms. Int J Pattern Recognit Artif Intell 1(2):273-302.
Le T, Paultre P (2013) Modal identification based on the time-frequency domain decomposition of unknown-input dynamic tests. Int J Mech Sci 71:41-50.
Li P, Abbott A, Schmoldt D (1996) Automated analysis of CT images for the inspection of hardwood log. Pages 1744-1749 *in* Proc. IEEE Conference on Neural Networks. June 3-6, 1996, Washington, DC.
Mallat S (1999) A wavelet tour of signal processing, 2nd edition. Academic Press, New York, NY.
Murphy G, Cown D (2015) Sand, stem and log segregation based on wood properties: a review. Scand J Fr Res 30(8): 757-770.
NHLA (2015) Rules for the measurement and inspection of hardwood and cypress. National Hardwood Lumber Association, Memphis, TN. 104 pp.
Ross RJ, McDonald KA, Green DW, Schad KC (1997) Relationship between log and lumber modulus of elasticity. Forest Prod J 47(2):89-92.
Slavič J, Simonovski I, Boltežar M (2003) Damping identification using a continuous wavelet transform: Application to real data. J Sound Vibrat 262:291-307.
Staszewski WJ (1997) Identification of damping in MDOF systems using time-scale decomposition. J Sound Vibrat 203(2):283-305.
Thomas L, Mili L, Thomas RE, Shaffer CA (2006) Defect detection on hardwood logs using laser scanning. Wood Fiber Sci 38(4):682-695.
Thomas RE, Thomas L, Shaffer C (2008) Defect detection on hardwood logs using high-resolution laser scan data. Pages 163-167 *in* Proc. 15th International Symposium on Nondestructive Testing of Wood, September 10-12, 2007, Duluth, MN. Natural Resources Research Institute, University of Minnesota, Duluth, MN.
Tiitta M, Biernacki JM, Beall FC (1998) Acousto-ultrasonic assessment of internal decay in glulam beams. Wood Fiber Sci 30:24-37.
Ülker-Kaustell M, Karoumi R (2011) Application of the continuous wavelet transform on the free vibrations of a steel-concrete composite railway bridge. Eng Struct 33: 911-919.
Wagner F, Taylor F, Ladd D, McMillin C, Roder F (1989) Ultrafast CT scanning of an oak log for internal defects. Forest Prod J 39(11/12):62-64.
Wang X (2013) Acoustic measurements on trees and logs: A review and analysis. Wood Sci Technol 47:965-975.
Wang X, Carter P, Ross RJ, Brashaw BK (2007) Acoustic assessment of wood quality of raw forest materials—A path to increased profitability. Forest Prod J 57(5):6-14.
Wang X, Stelzer HE, Wiedenbeck J, Lebow PK, Ross RJ (2009) Assessing wood quality of borer-infested red oak logs with a resonance acoustic technique. Wood Fiber Sci 41(2):180-193.
Wang X, Verrill S, Lowell E, Ross RJ, Herian VL (2013) Acoustic sorting models for improved log segregation. Wood Sci Technol 45(4):343-352.
Wiedenbeck J, Wiemann M, Alderman D, Baumgrass J, Luppold W (2003) Defining hardwood veneer log quality attributes. General Technical Report NE-313. U.S. Department of Agriculture, Forest Service, Northeastern Research Station, Newtown Square, PA. 36 pp.

APPENDIX: DETERMINATION OF INSTANTANEOUS FREQUENCY AND DAMPING RATIO BASED ON CONTINUOUS WAVELET TRANSFORM

CONCEPT OF CONTINUOUS WAVELET TRANSFORM

Wavelet transform (WT) is a localized decomposition in time-scale (frequency) domain, and its essence is to represent or approximate a signal by using a family of basic functions, allowing local features of the signal to be better represented. The CWT of a finite energy signal $x(t) \in L^2(R)$ can be defined as follows (Mallat 1999):

$$W[x](a,b) = \frac{1}{\sqrt{a}} \int_{-\infty}^{+\infty} x(t)\varphi^*\left(\frac{t-b}{a}\right)\mathrm{d}t, \qquad (1)$$

where $\varphi^*(\cdot)$ is the complex conjugate of the basic wavelet function $\varphi(\cdot)$, and a and b are the translation and scale/dilation parameters, respectively (Grossmann and Morlet 1984; Slavič et al 2003). The wavelet coefficients $W[x](a,b)$ are normalized by the factor $1/\sqrt{a}$. This normalization ensures that the integral energy given by each wavelet $\varphi_{a,b}(\cdot)$ is independent of the dilation a.

The most common wavelet for analyzing transient free vibration signals is the Morlet wavelet (Kronland-Martinet et al 1987; Staszewski 1997). In this report, the modified Morlet wavelet was used to estimate the damping ratio of the acoustic signals. A modified Morlet is defined as

$$\varphi(t) = \frac{1}{\sqrt{\pi f_b}} e^{j2\pi f_c t} e^{-t^2/f_b}, \tag{2}$$

where f_b is the wavelet bandwidth parameter and f_c is wavelet center frequency. The center frequency f_c of the Morlet wavelet is approximately bounded by $2\pi f_c \geq 5$ to fulfill the condition of admissibility (Kronland-Martinet et al 1987). The Fourier transform of the Morlet wavelet is

$$\hat{\varphi}(af) = e^{-\pi^2 f_b (af - f_c)^2}. \tag{3}$$

ASYMPTOTIC ANALYSIS

For a certain class of wavelets, referred to as the analytic wavelets, the analysis procedure can be much simplified if the signal is the asymptotic function. The characteristic of an analytic function $f(t)$ is that its Fourier transform values are all zeros in terms of the negative frequencies, namely

$$\hat{f}(\omega) = 0, \ \forall \omega < 0. \tag{4}$$

A common monochromatic signal can be described as a function of an instantaneous amplitude $A(t)$ and a phase $\varphi(t)$ as follows (Delprat et al 1992; Ülker-Kaustell and Karoumi 2011):

$$x(t) = A(t)\cos(\phi(t)). \tag{5}$$

The instantaneous angular frequency can be defined as the time derivative of the phase

$$\omega(t) = \dot{\phi}(t). \tag{6}$$

If variation of the amplitude $A(t)$ is much smaller than that of the phase $\varphi(t)$, ie if the following condition can be met

$$\left|\dot{\phi}(t)\right| \gg \left|\frac{\dot{A}(t)}{A(t)}\right|, \tag{7}$$

then, the signal $x(t)$ is called an asymptotic signal. In this condition, the associated analytic signal of $x(t)$ can be approximated by the following form:

$$Z_x(t) \approx A(t) e^{j\phi(t)}. \tag{8}$$

If the signal is asymptotic and wavelet function is analytic, the relationship between the CWT of the real-valued signal $x(t)$ and that of its analytic signal $Z_x(t)$ can be denoted by

$$W[x](a,b) = \frac{1}{2} W[Z_x](a,b). \tag{9}$$

An approximation of the CWT is proposed as follows by using Taylor's formulae around $t = b$ (Carmona et al 1998; Le and Paultre 2013):

$$\begin{aligned} W[x](a,b) &= \frac{1}{2} W[Z_x](a,b) \\ &= \frac{1}{2\sqrt{a}} \int_{-\infty}^{\infty} A(t) e^{j\phi(t)} \varphi^*\left(\frac{t-b}{a}\right) dt \\ &\approx \frac{\sqrt{a}}{2} A(b) e^{j\phi(b)} \hat{\varphi}^*\left(a\dot{\phi}(b)\right). \end{aligned} \tag{10}$$

WAVELET RIDGE AND SKELETON OF CWT

Assuming that a signal consists of only a frequency component, the maximum modulus of its CWT is concentrated along a curve in the time–frequency plane, which is referred to as wavelet ridge $a_r(b)$. The maximum modulus corresponding to the points located in the curve is called wavelet skeleton $W[x](a_r(b), b)$. Because the wavelet used in this study is analytic, a definition of the wavelet ridge and its skeleton are given as follows:

$$\begin{cases} a_r(b) = \dfrac{\omega_{\varphi_0}}{\dot{\phi}(b)} \\ W[x](a_r(b), b) \approx \dfrac{\sqrt{a}}{2} A(b) e^{j\phi(b)} \hat{\varphi}^*\left(a_r(b)\dot{\phi}(b)\right), \end{cases} \tag{11}$$

where ω_{φ_0} is the angular frequency at which the modulus of the mother wavelet obtains the local maximum. Thus, the amplitude of the asymptotic signal $A(b)$ can be determined by the modulus of wavelet ridge using the following equation:

$$A(b) = \frac{|W[x](a_r(b), b)|}{\left|\frac{\sqrt{a}}{2} e^{j\phi(b)} \hat{\varphi}^*\left(a_r(b)\dot{\phi}(b)\right)\right|} = \frac{2|W[x](a_r(b), b)|}{\sqrt{a}\left|\hat{\varphi}^*\left(a_r(b)\dot{\phi}(b)\right)\right|}. \quad (12)$$

If a signal $x(t)$ consists of multiple frequency components, ie $x(t) = \sum_k x_k(t)$, because of the linearity property of CWT, its CWT can be processed by

$$W[x](a, b) = W\left[\sum_k x_k(t)\right](a, b) = \sum_k W[x_k](a, b). \quad (13)$$

By appropriately selecting the mother wavelet parameters, each particular component of $x(t)$ can be extracted from the multicomponents and each modulus of CWT of the point on the ridge is local maximum in the case.

ESTIMATION OF INSTANTANEOUS FREQUENCY AND DAMPING RATIO

For a linear n-degree-of-freedom system, when the kth point of the system is impacted by a unit impulse force, the response at the ith point can be represented as

$$h_{lk}(t) = \sum_{i=1}^{n} \frac{\phi_i^l \phi_i^k}{m_i f_{di}} e^{-2\pi\zeta_i f_i t} \sin(2\pi f_{di} t), \quad (14)$$

where ϕ_i^l and ϕ_i^k are the ith-order modal shape of the testing point l and k, respectively, m_i is the ith-order modal mass, ζ_i is damping ratio of the ith-order modal shape, f_i is the ith-order undamped frequency, and $f_{di} = \sqrt{1-\zeta_i^2} f_i$ is the ith-order damped frequency.

To facilitate the expression, the response signal can be expressed as

$$x(t) = \sum_{i=1}^{n} A_i e^{-2\pi\zeta_i f_i t} \sin(2\pi f_{di} t), \quad (15)$$

where $A_i = \frac{\phi_i^l \phi_i^k}{m_i f_{di}}$ is a constant only related to the testing point and modal order i.

When the modified Morlet wavelet transform is applied to the response function $x(t)$, the following equation can be obtained according to Eqs (3), (10), and (15)

$$W[x](a, b) \approx \frac{\sqrt{a}}{2} \sum_{i=1}^{n} A(b) e^{j\phi(b)} \hat{\varphi}^*\left(a\dot{\phi}(b)\right) = \frac{\sqrt{a}}{2} \sum_{i=1}^{n} A_i e^{-2\pi\xi_i f_i b} e^{-\pi^2 f_b (a f_i - f_c)^2} e^{j(2\pi f_{di} b)}, \quad (16)$$

where $e^{-\pi^2 f_b (a f_i - f_c)^2}$ is a dilated version of Fourier transform of the Morlet wavelet. For a fixed value of the dilatation parameter $a = a_i = f_c/f_i$, $e^{-\pi^2 f_b (a f_i - f_c)^2}$, wavelet modulus can reach the maximum (skeleton) on the wavelet ridge. In this case, the ith-order mode associated with a_i dominates the wavelet transform, whereas all the other terms contribute nothing to the wavelet modulus and therefore are negligible. Thus, the wavelet transform of each separated mode i can be represented as

$$W[x](a_i, b) = \frac{\sqrt{a_i}}{2} A_i e^{-2\pi\zeta_i f_i b} e^{j(2\pi f_{di} b)}. \quad (17)$$

For an idiomatic expression, we substitute t for b in Eq (17); thus, the equation can be rewritten as

$$W[x](a_i, t) = \frac{\sqrt{a_i}}{2} A_i e^{-2\pi\zeta_i f_i t} e^{j(2\pi f_{di} t)} = B_i(t) e^{j\phi_i(t)}. \quad (18)$$

The instantaneous amplitude $B_i(t)$ and the instantaneous phase $\phi_i(t)$ of the CWT coefficient $W[x](a_i, t)$ can be defined as

$$\begin{cases} B_i(t) = \dfrac{\sqrt{a_i}}{2} A_i e^{-2\pi\zeta_i f_i t} \\ \phi_i(t) = 2\pi f_{di} t \end{cases} . \quad (19)$$

The following equation can be obtained by taking the derivatives of Eq (19):

$$\begin{cases} \dfrac{\mathrm{d}\ln B_i(t)}{\mathrm{d}t} = \dfrac{1}{B_i(t)} \dfrac{\mathrm{d}B_i(t)}{\mathrm{d}t} = -2\pi\zeta_i f_i \\ \dfrac{\mathrm{d}\phi_i(t)}{\mathrm{d}t} = 2\pi f_{di} = 2\pi f_i \sqrt{1-\zeta_i^2} \end{cases} . \quad (20)$$

The instantaneous frequency f_i and damping ratio ζ_i of the system can be derived by solving Eq (20).